Cell Host & Microbe
Article

Type I Interferon Imposes a TSG101/ISG15 Checkpoint at the Golgi for Glycoprotein Trafficking during Influenza Virus Infection

Sumana Sanyal,[1] Joseph Ashour,[1] Takeshi Maruyama,[1] Arwen F. Altenburg,[1] Juan Jose Cragnolini,[1] Angelina Bilate,[1] Ana M. Avalos,[1] Lenka Kundrat,[1] Adolfo García-Sastre,[3,4,5] and Hidde L. Ploegh[1,2,*]
[1]Whitehead Institute for Biomedical Research, 9 Cambridge Center, Cambridge, MA 02142, USA
[2]Department of Biology, Massachusetts Institute of Technology, Cambridge, MA 02139, USA
[3]Department of Microbiology, Mount Sinai School of Medicine, 1 Gustave L. Levy Place, New York, NY 10029, USA
[4]Department of Medicine, Mount Sinai School of Medicine, 1 Gustave L. Levy Place, New York, NY 10029, USA
[5]Global Health and Emerging Pathogens Institute, Mount Sinai School of Medicine, 1 Gustave L. Levy Place, New York, NY 10029, USA
*Correspondence: ploegh@wi.mit.edu
http://dx.doi.org/10.1016/j.chom.2013.10.011

SUMMARY

Several enveloped viruses exploit host pathways, such as the cellular endosomal sorting complex required for transport (ESCRT) machinery, for their assembly and release. The influenza A virus (IAV) matrix protein binds to the ESCRT-I complex, although the involvement of early ESCRT proteins such as Tsg101 in IAV trafficking remain to be established. We find that Tsg101 can facilitate IAV trafficking, but this is effectively restricted by the interferon (IFN)-stimulated protein ISG15. Cytosol from type I IFN-treated cells abolished IAV hemagglutinin (HA) transport to the cell surface in infected semi-intact cells. This inhibition required Tsg101 and could be relieved with deISGylases. Tsg101 is itself ISGylated in IFN-treated cells. Upon infection, intact Tsg101-deficient cells obtained by CRISPR-Cas9 genome editing were defective in the surface display of HA and for infectious virion release. These data support the IFN-induced generation of a Tsg101- and ISG15-dependent checkpoint in the secretory pathway that compromises influenza virus release.

INTRODUCTION

The assembly and release of enveloped viruses is a multistep process that requires host factors and is often hijacked by the virus in order to execute membrane remodeling and budding. The most well-characterized are retroviruses, which exploit the cellular endosomal sorting complex required for transport (ESCRT) machinery for budding (Martin-Serrano and Neil, 2011). The matrix protein of many such viruses contains a late-domain sequence (PTAP or L domain) that binds to components of the ESCRT machinery typically involved in the formation of vesicles into multivesicular bodies. Influenza viruses, on the other hand, are believed to have evolved an ESCRT-independent mode of budding, but the exact mechanism of influenza virus assembly and budding is not clear. The consensus is that the coat proteins initiate the process. Hemagglutinin (HA) and neuraminidase associate with the virus matrix protein M1 at lipid microdomains followed by the recruitment of M2—an ion channel capable of altering membrane curvature (Rossman et al., 2010). Mutations introduced into the amphipathic helix of M2 abolish membrane scission and virus release (Rossman and Lamb, 2011; Rossman et al., 2010). Although influenza lacks a conventional L domain, the matrix protein M1 binds to the ESCRT-I complex, suggesting a possible role in assembly (Bruce et al., 2009). Budding of filamentous and nonfilamentous influenza A requires neither VPS4 nor VPS28 (Bruce et al., 2009). However, the involvement of early ESCRT proteins such as Tsg101 in intracellular trafficking of IAV remains to be demonstrated directly.

Host cells impose restrictions on various steps in the virus life cycle, including entry, replication, assembly, and release. Antiviral mechanisms are launched by the induction of type I interferon (IFN-I) in the infected cell. ISG15 is one of the most abundantly expressed genes upon IFN-I signaling, and it has general antiviral effects (Skaug and Chen, 2010; Zhao et al., 2010). Retrovirus release is blocked upon IFN-I treatment or by exogenous expression of ISG15 (Seo and Leis, 2012; Zhao et al., 2013). ISG15 knockout mice ($ISG15^{-/-}$) show increased susceptibility to a number of virus infections, including influenza (Hsiang et al., 2009). The expression of ISG15 blocks the budding of a number of viruses through the conjugation of ESCRT components that are employed during virus infections. For example, the budding of Ebola virus-like-particle is blocked by ISG15 through the inhibition of Nedd4 ligase activity; HIV-1 budding is impaired upon IFN induction because of a loss of Tsg101 binding to the HIV Gag protein. Although the nonstructural protein 1 (NS1) of influenza B virus directly binds to and antagonizes the activity of ISG15, this is not the case for influenza A virus (Zhao et al., 2013; Yuan and Krug, 2001; Hsiang et al., 2009).

Here, we use a biochemical assay based on the use of perfringolysin O (PFO)-perforated semi-intact cells to study flu biogenesis. This preparation faithfully recapitulates intracellular glycoprotein trafficking and virus release. PFO is a cholesterol-binding, pore-forming toxin that selectively perforates the plasma membrane while leaving intracellular organelles intact. Thus, we can manipulate the composition of the cytoplasm as well as deliver otherwise cell-impermeable reagents such as the nonhydrolysable GTP analog GTPγS in order to determine

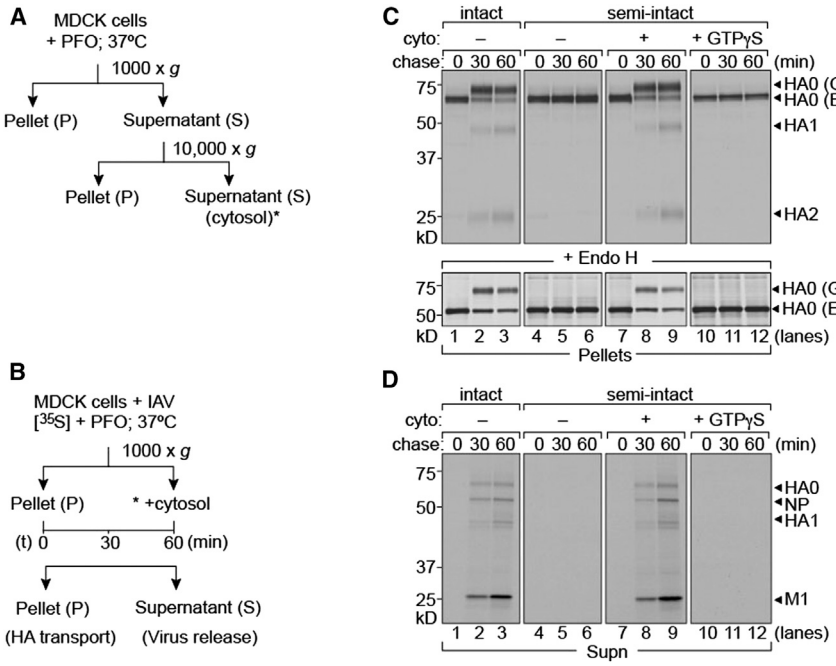

Figure 1. Trafficking of IAV in Semi-Intact Cells Requires Added Cytosol

1 × 10^6 MDCK cells were infected with influenza A/WSN/33 at a multiplicity of infection (MOI) of ~0.5 for 5 hr and radiolabeled with [^{35}S]cysteine/methionine. Cells were left intact or permeabilized with 100 nM PFO, supplemented with concentrated MDCK cytosol, and chased for 30 and 60 min. At each time point, pellet and supernatant fractions were separated by centrifugation.

(A and B) Experimental setup.

(C) Top: pellet fractions were lysed and immunoprecipitated with anti-HA IgG2b on protein G beads. Pulse-chase experiments on intact cells (lanes 1–3). Semi-intact cells supplemented with MDCK cytosol (lanes 7–9). Absence of exogenous cytosol or addition of GTPγS arrests HA in the ER (lanes 10–12). Bottom: EndoH digested HA in the pellet fractions.

(D) Supernatant fractions from intact or permeabilized cells were treated with chicken erythrocytes in order to isolate intact virions. Release of virus particles occurred in intact cells (lanes 1–3) and semi-intact cells supplemented with cytosol (lanes 7–9).

their effect on cytosol-dependent intracellular trafficking events. Exogenous cytosol from various sources can be delivered to these semi-intact cells through a mild osmotic shock. We previously used this preparation to measure ATP-dependent transport of misfolded glycoproteins from the endoplasmic reticulum (ER) to the cytosol as part of a protein quality control system (Ernst et al., 2011; Sanyal et al., 2012). Now, we have extended this approach to understand intracellular protein trafficking routes upon IFN induction during influenza virus infection and to identify cytosolic components relevant for the process. We show that semi-intact cells support virus assembly and release with kinetics comparable to those of intact cells. We identified Tsg101 as a component essential for the post-Golgi trafficking of HA to the plasma membrane (PM) prior to the budding of the virus and find that Tsg101 is ISGylated upon the exposure of cells to IFN, providing a plausible link between IFN exposure and interference with glycoprotein trafficking. Cas9-CRISPR-mediated inactivation of Tsg101 yielded cells refractory to infection, possibly because of defects in virus entry, thus underscoring the advantage of using semi-intact cells to resolve virus entry, assembly, and release processes. Both the use of semi-intact cells and the generation of a knockout cell line establish the involvement of Tsg101 upon IFN induction and influenza infection. Endogenous glycoprotein transport acquires a pronounced dependency on Tsg101 in IFN-I-treated cells, which is negatively regulated by ISG15 and exploited by IAV during infection.

RESULTS

Trafficking of IAV in Semi-Intact Cells Requires Exogenous Cytosol

To demonstrate trafficking and budding of IAV in PFO-permeabilized cells, we infected Madin-Darby canine kidney (MDCK) cells with influenza A/WSN/33 for 5 hr. Then, cells were pulse labeled with [^{35}S]cysteine/methionine for 10 min, treated with PFO at 0°C, washed briefly in order to remove excess PFO, and transferred to 37°C in order to initiate permeabilization of the PM. This approach allowed us to track the fate of the wave of only newly synthesized viral proteins while ignoring the contribution of unlabeled virus particles poised for release at the time of perforation. The same strategy of cell permeabilization, performed in a small volume in order to minimize dilution, yielded concentrated cytosol (Figure 1A). We incubated PFO-treated cells with cytosol from MDCK cells at 37°C for the indicated times. At each time point, the supernatant and the pellet fractions were separated by centrifugation. Pellet fractions were lysed in NP40-containing lysis buffer and treated with anti-HA antibodies immobilized on protein G beads in order to recover HA. In order to isolate intact virions released from the PFO-treated cells, supernatants were adsorbed onto chicken erythrocytes, which capture viral particles via the sialic acids on the erythrocytes (Figure 1B). Then, the material was visualized by SDS-PAGE and autoradiography.

First, we measured intracellular trafficking of HA from the ER to the Golgi and from there to the PM in semi-intact cells by monitoring the maturation of N-linked glycans on HA (Figure 1C). The ER-resident, high-mannose form of HA can be distinguished from its Golgi counterpart by its distinct mobility on SDS-PAGE and by the sensitivity of the former to treatment with endoglycosidase H (EndoH) (Figure 1C, bottom). The inclusion of trypsin in the incubation medium allowed an assessment of the appearance of HA at the cell surface through formation of HA1 and HA2—the trypsin-cleavage products of HA0. Access of trypsin to the cytosol cannot result in the conversion of intracellular HA0 into HA1 and HA2 because the cleavage site in HA0 is lumenally disposed and, therefore, not accessible to added protease even when it enters perforated cells. In the absence of added cytosol, intracellular transport of HA ceased (Figure 1C). Kinetics of intracellular transport and surface display of HA in semi-intact

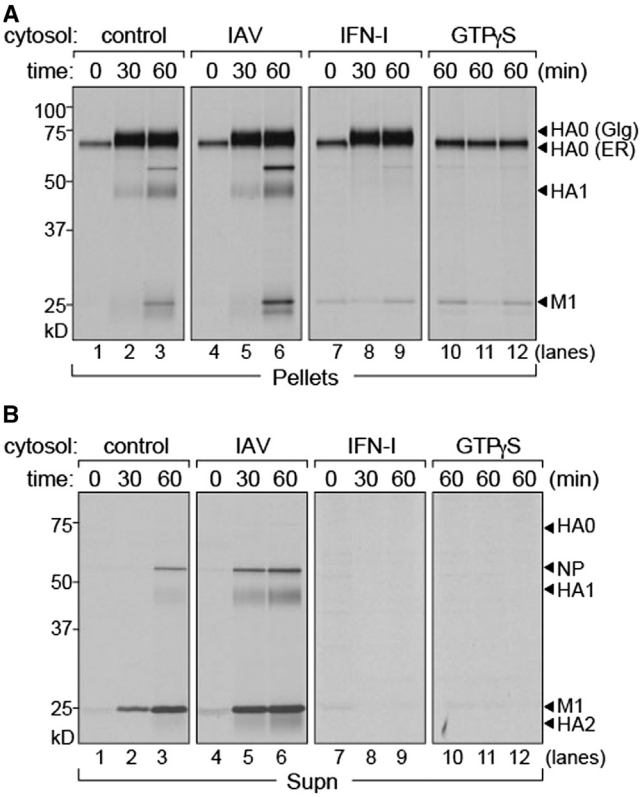

Figure 2. Cytosol from IAV-Infected and IFN-I-Treated Cells Have Distinct Effects on Virus Release from Semi-Intact Cells

1×10^6 MDCK cells were infected with influenza A/WSN/33 at an MOI of ~0.5 for 5 hr and radiolabeled with [^{35}S]cysteine/methionine. Permeabilized cells were supplemented with (1) concentrated MDCK cytosol, (2) MDCK cytosol from IAV-infected cells, and (3) MDCK cytosol treated with IFN-I and chased for 30 and 60 min. At each time point, pellet and supernatant fractions were separated by centrifugation.

(A) Pellet fractions were lysed and immunoprecipitated with anti-HA IgG2b on protein G beads. Control cytosol (lanes 1–3) and cytosol from IAV-infected MDCK cells (lanes 4–6). Cytosol from IFN-treated MDCK cells (lanes 7–9) does not support HA transport from the Golgi to the PM. Cytosol supplemented with GTPγS (lanes 10–12).

(B) Supernatant fractions from permeabilized cells were treated with chicken erythrocytes in order to isolate intact virions. Release of virus particles with control cytosol (lanes 1–3) and cytosol from IAV-infected cells (lanes 4–6) with IFN-treated cytosol (lanes 7–9) or GTPγS-supplemented cytosol (lanes 10–12). See also Figure S1.

cells supplied with cytosol were comparable to those in intact cells, as measured by conversion of HA's high-mannose glycans to the complex type and the appearance of HA1 and HA2. The inclusion of GTPγS abolished transport from the ER to Golgi, which was anticipated because of its inhibition of coat protein II mediated vesicular transport (Lee and Miller, 2007). The inclusion of GTPγS is an important control that establishes quantitative permeabilization; residual intact cells would have supported HA maturation. In parallel with transport and surface arrival of HA, semi-intact cells supplemented with concentrated MDCK cytosol released intact virus or virus-like particles recovered by adsorption to chicken red blood cells (Figure 1D). The omission of cytosol or inclusion of GTPγS blocked the release of virus particles. Thus, semi-intact cells support virus assembly and release when supplemented with cytosol from a compatible exogenous source and do so at rates comparable to those seen in intact cells. The composition of the released particles—as assessed by SDS-PAGE and autoradiography—is indistinguishable for intact and cytosol-supplemented semi-intact cells.

Cytosol from IAV-Infected and IFN-I-Treated Cells Have Distinct Effects on Virus Release

We hypothesized that IAV infection induces host factors in the cytosol that modulate virus assembly and budding. Mammalian cells respond to virus infection by producing IFN-I, which, in turn, induces the expression of host factors with antiviral properties, a process that takes several hours. Viruses have evolved countermeasures for inducing host genes that facilitate virus trafficking and release either directly or by the modification of the existing sets of proteins while downregulating the expression of genes that compromise infection. To recapitulate such a physiological cytosolic environment, we used two different sources of cytosol: we extracted cytosol from MDCK cells that had either been infected with IAV or treated with IFN-I. Cytosol obtained from IAV-infected cells soon after infection would contain host proteins that assist in virus assembly and release. On the other hand, cytosol extracted from cells treated with IFN-I would be enriched in host factors that contribute to an antiviral milieu. We supplied these extracts to IAV-infected radiolabeled cells, permeabilized using PFO as described above. Cytosol from uninfected MDCK cells was used as a control (Figure 2A). Neither the abundance of HA nor the kinetics of trafficking from the ER to the Golgi were affected by the provision of different cytosol preparations, relative to control cells. However, the arrival of HA at the cell surface, as measured by the cleavage of HA0 with the concomitant appearance of HA1 and HA2, was impaired by cytosol from IFN-treated cells (Figure 2A). We observed no impairment in particle release into the supernatants from semi-intact cells supplied with cytosol from IAV-infected cells (Figure 2B). The provision of cytosol from IFN-treated cells likewise abolished particle release. Therefore, cytosol from IFN-treated cells must contain proteins that prevent the arrival of HA at the cell surface and its subsequent incorporation into virions or must lack proteins necessary for this to occur. This block occurs after the acquisition of complex-type glycans. The fraction of viral proteins that appear in released virions is too low to result in a measurable accumulation of intracellular HA upon the inhibition of virus release. The release of virions seen upon supplementation with cytosol from IAV-infected cells appears to be a consequence of NS1-mediated inhibition of a restriction factor (Figure S1 available online).

ISG15 Inhibits a Late Step in IAV Glycoprotein Transport and Blocks Virus Release

ISG15 is an abundantly expressed gene induced immediately upon exposure to IFN-I. We hypothesized that the observed blockade in HA transport to the cell surface in IFN-I-exposed cytosolic extracts was due to the ISGylation of host components that, in their unmodified form, facilitate virus trafficking. Therefore, we expressed Ubp43 (a specific deISGylase) (Malakhov et al., 2002) or CCHFVL-Otu (L protein of Crimean-Congo hemorrhagic fever virus containing an ovarian tumor domain that antagonizes ISG15 activity) (Frias-Staheli et al., 2007) in

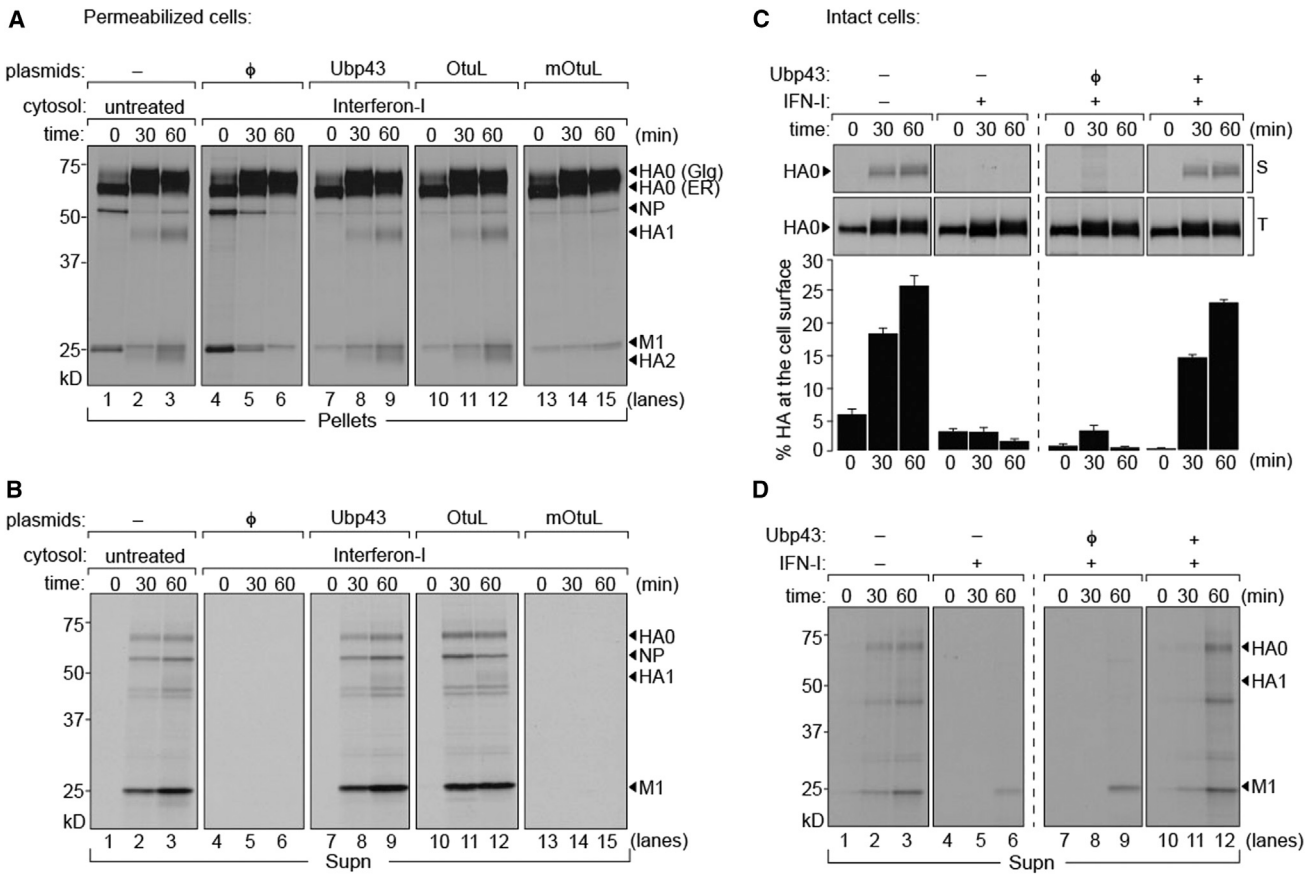

Figure 3. ISG15 Blocks a Late Step in Glycoprotein Transport

1×10^6 MDCK cells were infected with influenza A/WSN/33 at an MOI of ~0.5 for 5 hr and radiolabeled with [^{35}S]cysteine/methionine. Permeabilized cells were supplemented with (1) concentrated MDCK cytosol, (2) cytosol treated with IFN-I mixed with HEK 293T cytosol expressing an empty vector control, (3) IFN-I-treated cytosol mixed with Ubp43 expressed in HEK 293T cells, (4) IFN-I-treated cytosol mixed with CCHFVL-Otu (OtuL) expressed in HEK 293T cells, and (5) IFN-I-treated cytosol mixed with catalytically dead variant of CCHFVL-Otu (mOtuL) expressed in HEK 293T cells and chased for 30 and 60 min.

(A) Pellet fractions were lysed and immunoprecipitated with anti-HA IgG2b on protein G beads. Control cytosol (lanes 1–3), IFN-treated cytosol with empty control vector (lanes 4–6), and cytosol from IFN-treated cells mixed with Ubp43 (lanes 7–9), CCHFVL-Otu (lanes 10–12), or mutant CCHFVL-Otu (lanes 13–15).

(B) Supernatant fractions from permeabilized cells were treated with chicken erythrocytes in order to isolate intact virions. Virus particles released with control cytosol (lanes 1–3) or that from IFN-I treatment mixed with either Ubp43 (lanes 7–9) or CCHFVL-Otu (lanes 10–12). A block in release occurred with IFN-treated cytosol mixed with either control empty vector (lanes 4–6) or mutant CCHFVL-Otu (lanes 12–15).

(C) Intact A549 cells either mock-treated or treated with IFN-I for 8 hr (top left) were infected with HA-Srt virus (A/WSN/33 with a sortaggable HA) for 5 hr through a brief acid shock at pH 5, pulse labeled with [^{35}S]cysteine/methionine, and chased for the indicated time intervals. HA at the cell surface was biotinylated with sortase A and GGGK-biotin and isolated on NeutrAvidin beads, whereas total HA in the cell was immunoprecipitated on anti-HA antibodies. A549 cells transfected with either empty control vector or Ubp43 were IFN-I treated and infected with HA-Srt as above (top right). Surface HA was biotinylated, and total HA was immunoprecipitated on anti-HA antibodies. Bottom: the amount of HA reaching the cell surface was quantitated through densitometric analysis of the ratio of biotinylated HA to the total (intracellular + surface) HA ($[HA_{biotin}/HA_{total}] \times 100$). Error bars are from three independent experiments.

(D) Radiolabeled particles released into the media from intact A549 cells were adsorbed onto chicken erythrocytes and resolved by SDS-PAGE.

human embryonic kidney (HEK) 293T cells and prepared cytosol fractions by PFO treatment. Cytosol from IFN-I-treated cells was mixed with that of either Ubp43 or CCHFVL-Otu-containing cytosol in a 1:1 ratio and supplied to semi-intact cells in order to measure HA transport and virus production. An inactive mutant of CCHFVL-Otu served as a control. To control for the dilution of factors essential for transport, we mixed cytosol from IFN-treated cells with that of HEK 293T cells expressing an empty vector in a 1:1 ratio. The provision of this mixture inhibited the arrival of HA at the cell surface, indicating no loss of activity of the IFN-induced factors upon 2-fold dilution (Figure 3A). For cytosol from IFN-I-treated cells supplemented with either Ubp43 or CCHFVL-Otu, the transport of HA to the cell surface was restored, as judged from the appearance of HA1 and HA2. The catalytically inactive mutant of CCHFVL-Otu failed to relieve the inhibition observed upon the supply of cytosol from IFN-I-treated cells. These observations were corroborated by measuring the release of virus particles (Figure 3B). Block in virus release imposed upon IFN-I treatment was restored in samples incubated with either Ubp43 or CCHFVL-Otu, but not with inactive CCHFVL-Otu. Therefore, ISG15 must modify either a viral or host protein that inhibits a late step in the assembly of progeny virions and their subsequent release from cells.

To corroborate our findings in intact cells, we used the human lung epithelial cell line A549. We introduced either a control vector or an Ubp43 construct into these cells and treated them with IFN-I for 8 hr. Given that IFN-I treatment renders cells refractory to infection, we forced the fusion of virus (HA-Srt, multiplicity of infection of 1) at the plasma membrane by a brief exposure to pH 5.5 in order to deliver viral ribonucleoproteins (vRNPs) to the cytosol (White et al., 1981). The HA-Srt virus generated from A/WSN/33 contains an LPETG motif on its HA that can be selectively biotinylated with sortase A (Popp et al., 2012). Upon incubation (4 hr) in order to allow the synthesis of viral proteins, we performed a pulse-chase experiment. At each time point, cell-surface-displayed HA was biotinylated with sortase A and isolated on NeutrAvidin beads, whereas total HA was immunoprecipitated with anti-HA antibodies. We observed a block in the arrival of HA at the cell surface in IFN-I-treated cells that was restored in transfectants that express Ubp43 (Figure 3C). Supernatants released from these cells were adsorbed onto chicken erythrocytes and resolved by SDS-PAGE (Figure 3D). As observed with the surface appearance of HA, the release of intact virions was blocked upon IFN-I treatment and restored by the expression of Ubp43. The presence of radiolabeled M1 at the later time points in IFN-I-treated cells is most likely attributable to nonspecific adsorption due to the release of viral components by dying cells.

HA Transport to the Cell Surface Is Vps4 Independent but Tsg101 Dependent

An obvious target of ISGylation is the ESCRT machinery. Components of the ESCRT machinery, such as HIV-I, can be ISGylated and have been implicated in the budding of retroviruses (Martin-Serrano et al., 2001; Okumura et al., 2006). For the biogenesis of IAV, the involvement of the ESCRT complex was considered unlikely, given that a dominant-negative version of Vps4, an effector protein on which the ESCRT complexes converge, did not affect virus budding (Watanabe and Lamb, 2010). Instead, IAV budding is facilitated by M2, an ion channel equipped with an amphipathic helix that can alter membrane curvature (Chen et al., 2008; Rossman et al., 2010). We prepared cytosol from MDCK cells by permeabilization with PFO and depleted it of either Vps4 or Tsg101 (Figure 4A). Only trace amounts of Vps4 or Tsg101 remained, as verified by immunoblotting. Levels of GAPDH remained unchanged, verifying that depletion was specific. Cytosol that either contained Vps4 or had been depleted of Vps4 was applied to semi-intact cells infected with IAV in order to measure the trafficking of HA. Both Vps4-replete and Vps4-depleted cytosol supported the transport of HA to the cell surface (Figure 4B).

Tsg101 is a component of the ESCRT-I complex involved in the intracellular transport and assembly of a number of viruses such as HIV and Ebola (Martin-Serrano et al., 2001). To test the involvement of Tsg101 in transport and externalization of HA, we immunodepleted cytosol with anti-Tsg101 as described for Vps4 (Figure 4C). We delivered control and Tsg101-deficient cytosol to [^{35}S]cysteine/methionine semi-intact cells infected with IAV. Samples that received mock-depleted cytosol displayed unaltered kinetics of HA transport to the cell surface. Tsg101-depleted cytosol supported ER-to-Golgi transport, but not post-Golgi traffic of HA to the PM. Our results indicate that Tsg101 is required for HA to reach the cell surface from the Golgi network.

Next, we determined whether the Tsg101 dependence observed in infected cells also applies to cytosol from cells treated with IFN-I. Samples were supplemented with cytosol transduced with Ubp43 in order to relieve the transport of HA to the cell surface and tested in the presence or absence of Tsg101. Samples that received mock-depleted cytosol from IFN-I-treated cells supplemented with Ubp43 supported post-Golgi HA transport, whereas Tsg101-deficient extracts failed to do so regardless of the presence of Ubp43. GTPγS-supplemented cytosol was used as control for permeabilization. We conclude that intracellular traffic of HA relies on a Tsg101-dependent step and is sensitive to ISGylation. We examined the modification status of Tsg101 in transfectants that express HA-tagged ISG15. Covalent modification of Tsg101 with ISG15 was only observed in cells exposed to IFN-I, required for induction of the ISG15 conjugation apparatus, and reversed by cotransfection with the deISGylase Ubp43 (Figure 4D).

IFN-I Imposes a Block in the Transport of HA to the Cell Surface in Cas9-CRISPR-Mediated Tsg101 Knockout Cells

We generated Tsg101-deficient A549 cells using the Cas9-CRISPR method (Cong et al., 2013; Hwang et al., 2013; Mali et al., 2013) as well as siRNA-mediated knockdowns (data not shown). Although the ablation of Tsg101 is embryonically lethal (Wagner et al., 2003), we obtained several clones of Tsg101$^{-/-}$ A549 cells. These displayed reduced growth rates in comparison to wild-type (WT) cells but showed no gross morphological defects, as seen by light microscopy. We isolated five clones for which the deletion of Tsg101 was verified by immunoblotting of cell lysates (Figure 5A). Tsg101$^{-/-}$ cells showed no residual Tsg101 and were refractory to infection by IAV, possibly because of aberrations in the endocytic machinery imposed by the Tsg101 deficiency. This observation underscores the advantage of using semi-intact cells to separate entry and assembly defects that are otherwise difficult to identify in genome-wide screens applied to intact cells. In perforated cells, the only distinction between the two experimental settings is the presence or absence of Tsg101 from the delivered cytosol during these short incubations, all intracellular organelles being the same. Indeed, Tsg101 did not surface as a significant host factor in any of the published RNAi screens (Brass et al., 2009; Karlas et al., 2010; Shapira et al., 2009). To circumvent the resistance of Tsg101$^{-/-}$ cells to IAV infection through the standard endosomal entry pathway, we resorted to low-pH fusion of IAV in order to deliver vRNPs directly into the cytosol and performed a pulse-chase experiment. At each time point, surface-disposed HA was biotinylated with sortase A (Figure 5B, top). Total intracellular HA was immunoprecipitated with anti-HA antibodies (Figure 5B, bottom). We observed a complete block in the arrival of HA at the cell surface in Tsg101$^{-/-}$ cells, confirming our findings with permeabilized cells (Figure 5B). Likewise, the release of intact virions into the supernatant was blocked in Tsg101$^{-/-}$ cells, as observed by the absence of radiolabeled virus particles (Figure 5D). The inhibition and release

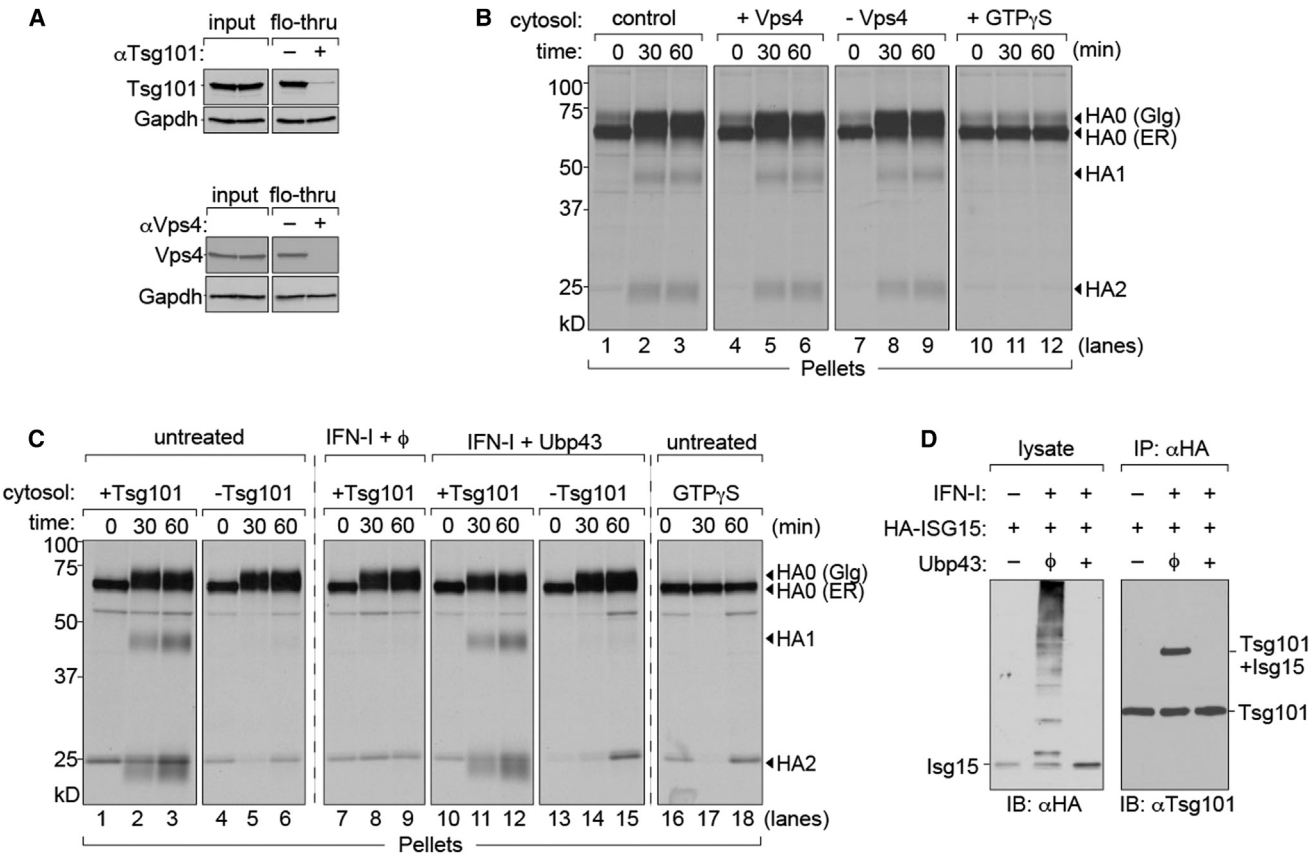

Figure 4. HA Transport to the Cell Surface Is Vps4 Independent but Tsg101 Dependent

(A) Immunodepletions from MDCK cytosol performed with anti-Vps4 or anti-Tsg101 antibodies on protein A beads. Beads without antibodies were used as control. Equivalent fractions of input and flowthrough were probed for Vps4 and Tsg101, respectively. GAPDH was used as a loading control in order to verify that depletion was specific.

(B) 1 × 10^6 MDCK cells were infected with influenza A/WSN/33 at an MOI of ~0.5 for 5 hr and radiolabeled with [^{35}S]cysteine/methionine. Cells were permeabilized with 100 nM PFO and supplemented with (1) concentrated MDCK cytosol, (2) MDCK cytosol treated with control beads, (3) cytosol depleted of Vps4, and (4) cytosol supplemented with GTPγS and chased for 30 and 60 min. Control cytosol (lanes 1–3), cytosol containing Vps4 (lanes 4–6), and cytosol lacking Vps4 (lanes 7–9). Cytosol supplemented with GTPγS (lanes 10–12).

(C) 1 × 10^6 MDCK cells were infected with influenza A/WSN/33 at an MOI of ~0.5 for 5 hr and radiolabelled with [^{35}S]cysteine/methionine. Permeabilized cells were supplemented with (1) either mock-depleted or Tsg101-deficient concentrated MDCK cytosol, (2) MDCK cytosol treated with IFN-I, (3) either mock-depleted or Tsg101-deficient MDCK cytosol treated with IFN-I mixed with Ubp43, and (5) cytosol supplemented with GTPγS and chased for 30 and 60 min. Untreated cytosol containing Tsg101 (lanes 1–3), and cytosol lacking Tsg101 (lanes 4–6). Cytosol from IFN-treated cells treated with Ubp43 containing Tsg101 (lanes 10–12) or Tsg101-deficient cytosol (lanes 13–15). Cytosol supplemented with GTPγS (lanes 16–18). Autoradiograms are representative of at least three independent experiments.

(D) HEK 293T cells were cotransfected with HA-ISG15 and either empty vector or Ubp43 delSGylase. Transfected cells were either untreated or treated with IFN-I for 6 hr (100 U/ml) and lysed in NP-40. Lysates were immunoblotted with anti-HA antibodies. ISGylated products were immunoprecipitated with anti-HA and probed with anti-Tsg101.

of infectious virus from Tsg101$^{-/-}$ cells was essentially complete, as confirmed by plaque assays (Figure 5C).

To identify the site at which the block in HA transport occurs, we prepared control and Tsg101$^{-/-}$ samples infected with IAV at low pH for 5 hr. Fixed and permeabilized cells were stained with TGN46 and anti-HA antibodies and examined by confocal microscopy (Figure 5E). In WT A549 cells, HA was distributed throughout the cell in a typical punctate pattern, whereas, in Tsg101$^{-/-}$ cells, HA was found in large accumulations that colocalized with the TGN network. Our results in Tsg101$^{-/-}$ cells, combined with those of permeabilized cells, show that Tsg101 plays a critical role in the transport of HA from the TGN to the plasma membrane.

Specific Host Proteins Traffic via Tsg101-Dependent Pathway upon IFN-I Induction

Tsg101-dependent transport of HA to the cell surface could be either specific for IAV proteins or a more general consequence of IFN-I exposure, which might affect other glycoproteins as well. We asked whether the trafficking of at least a subset of endogenous glycoproteins would display the same properties as that of HA upon IFN-I induction. We took advantage of two glycoprotein reporters, CD40L and transferrin receptor (TfR), both of which were engineered to contain an LPETG tag, which can be biotinylated on the surface of intact cells in a sortase A-catalyzed reaction (Popp et al., 2007, 2009). We generated MDCK cells that stably express either CD40L or TfR with an

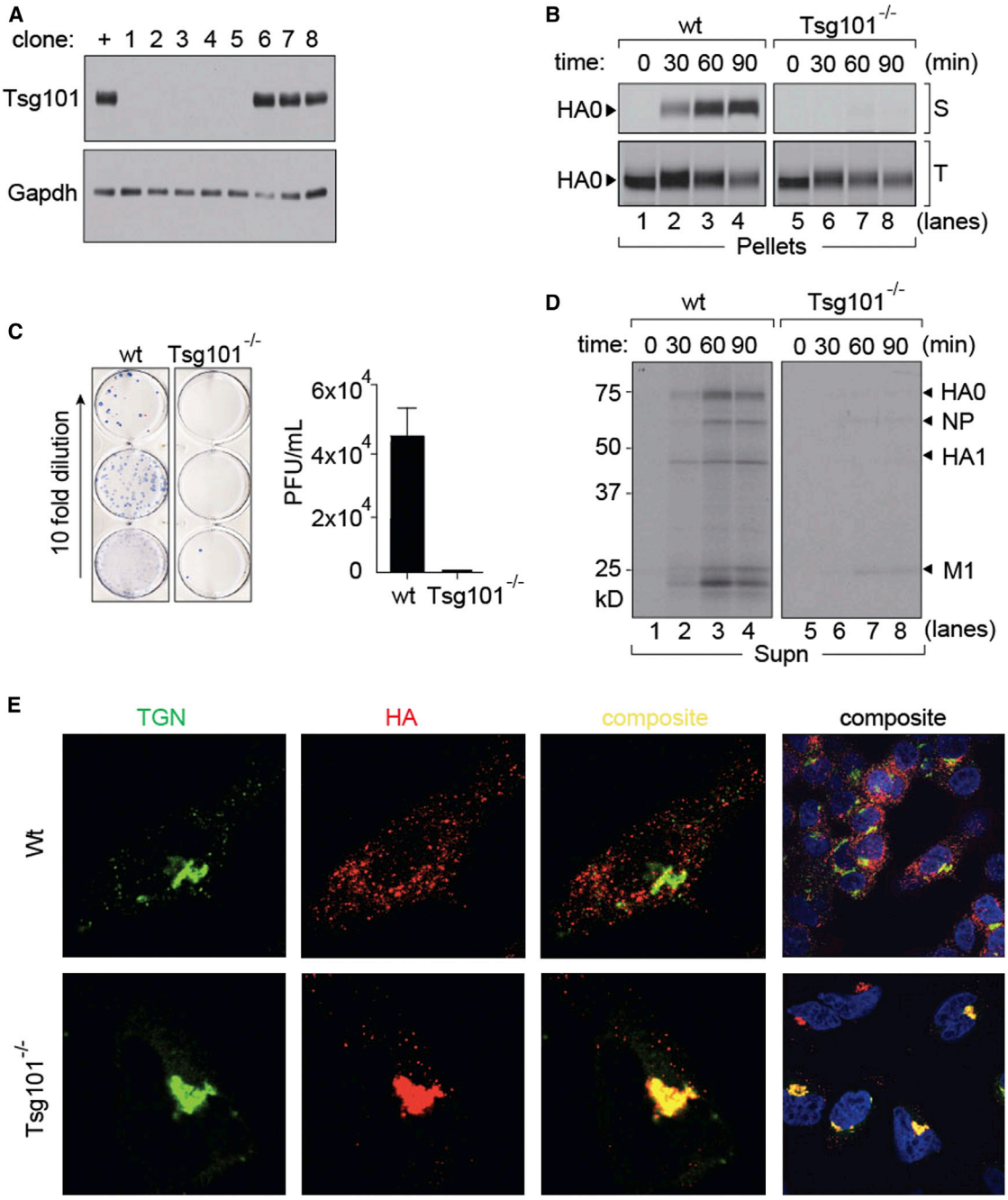

Figure 5. Cas9/CRISPR-Mediated Knockout of Tsg101 in A549 Cells

(A) Clonal isolates of A549 cells were immunoblotted for Tsg101 (+, control Tsg101-proficient cells; 1–9, different clonal isolates after limiting dilution).

(B) WT and Tsg101$^{-/-}$ cells were infected with HA-Srt for 5 hr at an MOI of 1 through a brief acid shock at pH 5.0 followed by pulse labeling with [^{35}S]cysteine/methionine for 10 min and chase for the indicated time intervals. At each time point, cell-surface HA was biotinylated with sortase A and GGGK-biotin and isolated on NeutrAvidin beads. The remaining intracellular HA was immunoprecipitated on anti-HA antibodies.

(C) Supernatants from infected (MOI = 1 at pH 5.0 for 4 hr) WT or Tsg101 knockout cells (three independent clones) were used to infect MDCK cells in 10-fold serial dilutions. MDCK cells were plated and overlaid with agar. After 2 days of infection, cells were stained with biotin-conjugated anti-NP single variable domain of heavy chain for visualization. Viral titers were quantitated from serial dilution of triplicates. Error bars represent mean ± SD.

(D) Radiolabeled particles released into the media from WT and Tsg101$^{-/-}$ were adsorbed onto chicken erythrocytes and resolved by SDS-PAGE.

(E) WT and Tsg101$^{-/-}$ A549 cells were infected with IAV (pH 5.0, MOI = 1) and incubated for 5 hr. Fixed and permeabilized cells were stained with anti-HA in order to identify virus particles and anti-TGN46 in order to define the trans-Golgi network. Images were acquired with a PerkinElmer spinning disk confocal microscope.

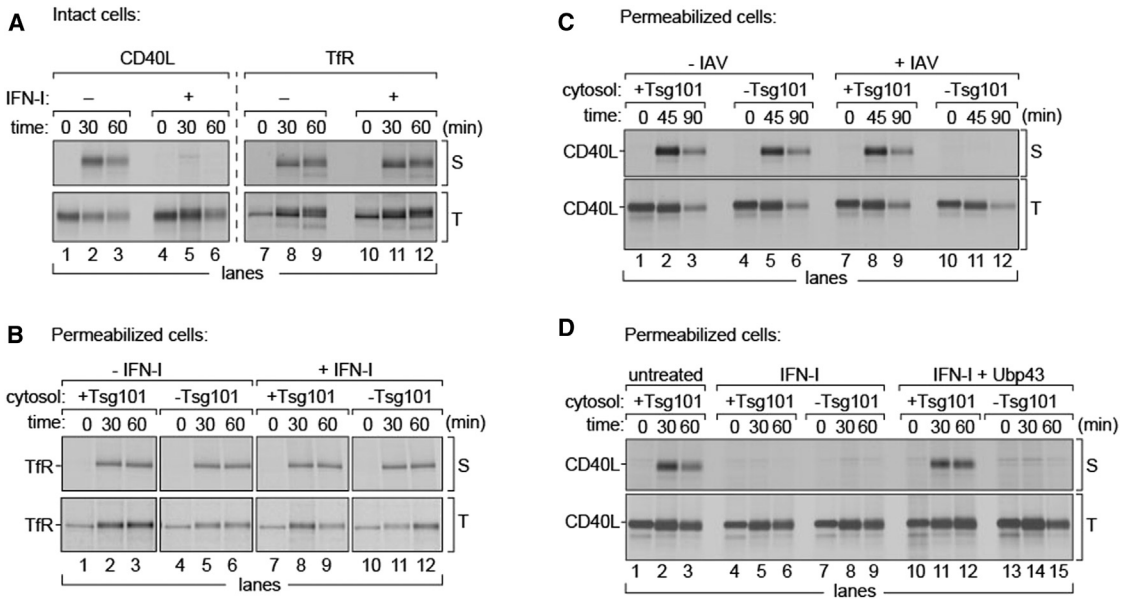

Figure 6. Tsg101-Dependent Transport of Endogenous Host Proteins

(A) MDCK cells stably expressing either CD40L or TfR were treated with IFN-I for 8 hr, radiolabeled with [^{35}S]cysteine/methionine for 15 min, and chased for the indicated time intervals. At each time point, surface-displayed CD40L or TfR were biotinylated. Total CD40L or TfR were immunoprecipitated on anti-HA beads.

(B) TfR-expressing cells were radiolabeled, permeabilized, and supplemented with (1) either Tsg101-replete or Tsg101-deficient untreated MDCK cytosol or (2) IFN-I-treated, Tsg101-replete, or Tsg101-deficient cytosol. At each time point, cell pellets were biotinylated with sortase A and GGGK-biotin and isolated on NeutrAvidin beads. Total TfR was immunoprecipitated on anti-HA beads.

(C) MDCK cells expressing CD40L were either mock infected or infected with influenza A/WSN/33 virus at an MOI of 0.5 for 5 hr and radiolabeled. Permeabilized cells were supplemented with Tsg101-replete or Tsg101-deficient cytosol. At each time point, pellets were treated with sortase A and GGGK-biotin for 1 hr on ice and immunoprecipitated on NeutrAvidin beads (S, surface-displayed). Intracellular CD40L was immunoprecipitated on immobilized HA beads (T, total). Uninfected cells (lanes 1–3 and 4–6). For flu-infected cells, transport of CD40L to the PM was abolished in the absence of Tsg101.

(D) CD40L-expressing cells were radiolabeled, permeabilized, and supplemented with (1) untreated MDCK cytosol; (2) IFN-I-treated, Tsg101-replete, or Tsg101-deficient cytosol; and (3) either Tsg101-replete or Tsg101-deficient IFN-I-treated, Ubp43-expressing cytosol. At each time point, pellets from these semi-intact cells were treated with sortase A and GGGK-biotin (S, surface-displayed) or lysed and immunoprecipitated on immobilized HA beads (T, total). Uninfected cells (lanes 1–3 and 4–6), IFN-I-treated cells in the presence or absence of Tsg101 (lanes 4–6 and 7–9), IFN-I-treated cytosol supplemented with Ubp43 in the presence of Tsg101 (lanes 10–12), and the absence of Tsg101 (lanes 13–15). Autoradiograms are representative of at least three independent experiments.

LPETG and HA epitope tag placed at their C terminus for the quantitation of total protein levels. First, we tested whether trafficking characteristics of these reporters were altered upon IFN-I induction. Intact MDCK cells expressing either CD40L or TfR were exposed to IFN-I for 8 hr, radiolabeled, and chased for various time intervals. Arrival at the cell surface was monitored through sortase A-catalyzed biotinylation. We observed a clear difference between transport characteristics of CD40L and TfR to the cell surface upon IFN-I treatment. Arrival of CD40L at the cell surface was abolished (Figure 6A), whereas that of TfR was unaffected (Figure 6A) by IFN-I treatment. To confirm these results, we measured the transport of TfR in permeabilized cells supplemented with cytosol from control or IFN-I-treated cells either proficient or deficient in Tsg101. Under all conditions, TfR transport to the cell surface was unaffected (Figure 6B).

To explore whether the defect in CD40L transport upon IFN-I treatment was also a Tsg101-dependent process, we tested whether the trafficking of CD40L was altered by virus infection. Transport of CD40L to the cell surface was monitored in IAV-infected samples and in mock-infected controls (Figure 6C). For both samples, cells were radiolabeled, permeabilized, and incubated with exogenous MDCK cytosol containing Tsg101 or immunodepleted of Tsg101. At 45 and 90 min, pellet fractions were collected, and the surface-disposed pool of CD40L was modified by sortase A-catalyzed biotinylation followed by immunoprecipitation on NeutrAvidin beads. Because the LPETG tag is lumenally oriented, it remains protected from sortase A unless exposed at the cell surface. Transport of CD40L to the surface and subsequent biotinylation was not affected in mock-infected control cells irrespective of Tsg101 status. However, surface exposure of CD40L in cells infected with IAV required Tsg101 (Figure 6C, top). Expression levels of CD40L remained constant for all samples (Figure 6C, bottom). We conclude that post-Golgi protein transport to the cell surface of CD40L becomes Tsg101-dependent during IAV infection.

Next, we tested whether the alteration of CD40L trafficking patterns was the result of an antiviral response that ensues upon virus infection. We used MDCK cells that stably express CD40L and radiolabeled them in a 15 min pulse. We permeabilized these cells and incubated them with cytosol from IFN-I-treated cells either Tsg101 replete or immunodepleted with anti-Tsg101 antibodies. At 30 and 60 min, pellet fractions were collected, and the surface-disposed fraction of CD40L was modified by sortase A-catalyzed biotinylation as described. Samples incubated with untreated MDCK cytosol supported CD40L transport and biotinylation at the cell surface (Figure 6D,

top). In the absence of any viral infection, but when supplying IFN-I-treated cytosol, transport of CD40L to the cell surface was compromised irrespective of the presence of Tsg101. Thus, results with CD40L recapitulate the characteristics of HA transport under IFN-I treatment, and CD40L presumably suffers a similar ISG15-imposed arrest. To relieve ISG15-mediated inhibition of transport, we prepared cytosol from IFN-I-treated cells and mixed it with Ubp43-containing cytosol (as described above) followed by immunodepletion of Tsg101. In cells that were incubated with cytosol from IFN-I-exposed cells supplemented with Ubp43, transport of CD40L to the cell surface was restored in the presence of Tsg101. Cytosol depleted of Tsg101 failed to support the appearance of CD40L at the cell surface. Total levels of CD40L remained constant, as detected by immunoprecipitation via the HA epitope (Figure 6D, bottom). We conclude that, upon treatment with IFN-I, CD40L trafficking patterns are altered such that they become dependent on Tsg101 and sensitive to ISGylation, whereas patterns of CD71 remain unaffected because of distinct routes of transport.

DISCUSSION

Cells exploit two major trafficking pathways for the internalization and export of cargo—the endocytic and the secretory pathways, respectively. Proteins destined for the extracellular environment enter the secretory pathway, mostly by cotranslational translocation into the ER and subsequent vesicular transport to the Golgi and, finally, to the cell surface. However, during viral or bacterial infections resulting in IFN induction, intracellular host protein trafficking routes must necessarily be altered in order to regulate cytokine secretion and the transport of other host proteins. Viral glycoproteins most likely possess intrinsic determinants for selecting sites of assembly, transport routes, and budding (Rossman and Lamb, 2011; Schmitt and Lamb, 2005). Among other host proteins typically involved in viral assembly, the family of proteins of the ESCRT machinery interact with the Gag and matrix proteins of a number of viruses, such as HIV and Ebola (Martin-Serrano et al., 2001; Jouvenet et al., 2011; Freed, 2004). These proteins include Tsg101 and those of the Nedd4 ligase family (Okumura et al., 2008). Tsg101 functions in the ESCRT-I complex as part of the vacuolar sorting machinery, where it helps select cargo for incorporation into vesicles that bud into multivesicular bodies (MVBs) (Razi and Futter, 2006). This process requires the formation of vesicles that bud away from the cytosol into the topological equivalent of extracellular space, a process essentially similar to virus budding at the PM (Hanson and Cashikar, 2012). Tsg101 is homologous to a ubiquitin E2-conjugating enzyme but lacks the ability to engage in ubiquitin transfer, notwithstanding its ability to interact tightly with ubiquitin.

Influenza viruses exit from discrete sites at the PM (Popp et al., 2012; Rossman and Lamb, 2011) enriched in cholesterol and sphingolipids. HA is the most abundant of the three envelope proteins, and critical determinants for lipid association are contained in its transmembrane domain (Ruigrok et al., 2000; Tafesse et al., 2013; Tsurudome et al., 1992). Because a mutant version of the AAA ATPase Vps4 devoid of enzymatic activity does not inhibit IAV release, the involvement of the ESCRT complex in IAV budding was considered unlikely (Bruce et al., 2009; Watanabe and Lamb, 2010). In addition, M2 alters membrane curvature in vitro, suggesting that the final step of membrane scission can be executed without the involvement of Vps4 (Rossman et al., 2010). Both intracellular transport and surface display of HA, as reconstituted here in semi-intact cells, support the lack of involvement of Vps4 in intracellular trafficking of HA or release of virus. In contrast, the depletion of Tsg101 abolishes HA transport to the cell surface and the subsequent release of virus. In the semi-intact cell system, Tsg101-deficient cytosol is added to infected, but otherwise normal, cells. Therefore, there is no reason to assume that the secretory pathway in these cells is massively defective, an argument supported by the ability to transport HA and allow the release of virus particles. Indeed, the provision of control cytosol is required to have transport proceed, whereas Tsg101-depleted cytosol is ineffective. Although the final stages of virus budding may indeed depend on M2, Tsg101 appears to play a critical role in the recruitment of HA to the cell surface prior to the release of IAV. Our demonstration that Tsg101 is itself ISGylated in IFN-treated cells provides a conceptual link between Tsg101's ability to orchestrate membrane trafficking and the consequences of IFN-I treatment on the intracellular movement of glycoproteins. Transport of an engineered CD40L shows a remarkable similarity to that of IAV HA, whereas an unrelated type II membrane protein (TfR) appears to follow a distinct trafficking route. The Tsg101-mediated mode of transport is either not active or redundant under normal physiological conditions, as confirmed by depletion from regular cytosol with no inhibitory effect on CD40L transport. The features of structure that confer this regulatory property on membrane proteins remain to be determined but do not easily segregate according to their type I or II transmembrane topology. We speculate that this property might extend to secreted proteins as well. Accordingly we propose that factors induced by IFN-I treatment differentially affect aspects of the secretory pathway, the details of which remain to be determined.

The M1 protein encoded by influenza A virus contains a putative late domain motif (YKRL) and interacts with the N-terminal ubiquitin E2 variant domain of Tsg101 (Diaz et al., 2009). M1 could facilitate influenza budding similar to the well-established interaction of HIV Gag or Ebola VP-40 with Tsg101. Virus infection of host cells elicits the production of IFN and presumably also attenuates or alters secretory activity. We speculate that transport vesicles are generated in a Tsg101-dependent fashion from the Golgi network, whereas the induction of IFN-I affects such trafficking (Figure 7). ISGylation of Tsg101, and possibly other components of the ESCRT machinery, would interfere with the normal operation of at least some of these transport pathways. The trafficking characteristics of CD40L and TfR upon IFN-I induction might depend on features of their transmembrane segments, requiring specific lipid-protein interactions, as observed for influenza HA and sphingomyelin (Tafesse et al., 2013). These transport vesicles may be akin to sorting endosomes or the ESCRT-dependent MVBs typically generated from late endosomes—a multisubunit complex with several components modified by ISG15. Hijacking of these transport vesicles by IAV with its glycoproteins anchored to the limiting membrane would allow arrival at the PM followed by M2-mediated budding. The operation of this trafficking route is partially supported by the finding that Rab11—a protein enriched in the TGN and recycling endosomes and MVBs—is required for IAV

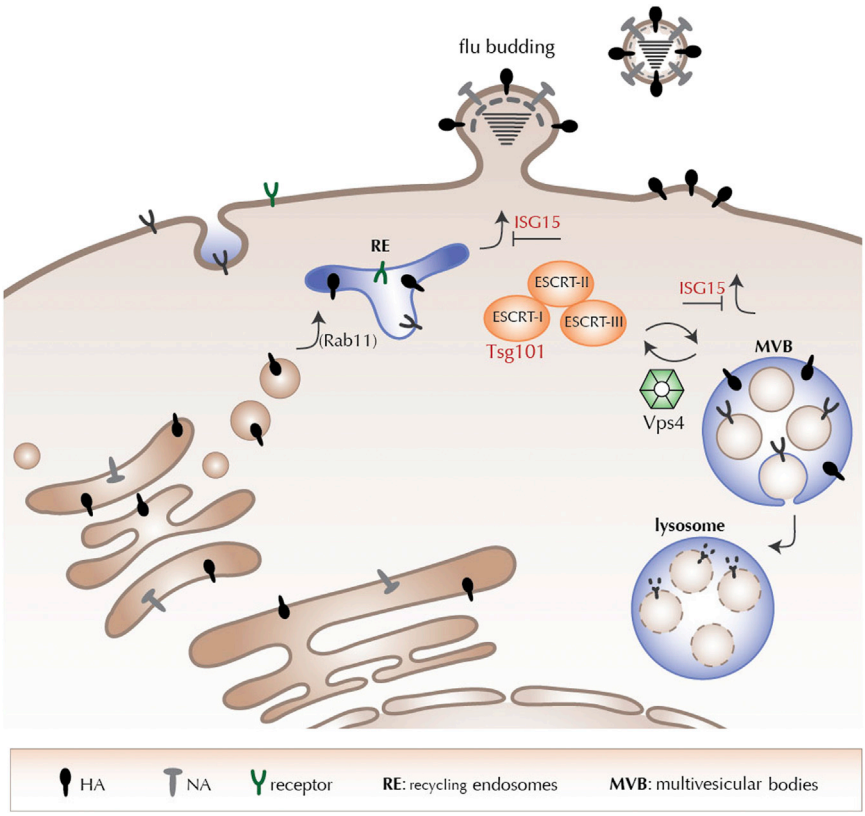

Figure 7. Proposed Model for Intracellular Influenza Trafficking and Budding

Proteins destined for the cell surface are synthesized at ER-bound ribosomes and traffic through the secretory pathway to arrive at the extracellular space. Influenza virus infection results in the induction of IFNα and IFNβ, which, in turn, create an antiviral state in the host cell by regulating gene expression and protein translation. Tsg101 functions as part of the ESCRT complex to form multivesicular bodies; the induction of IFNs activates an ISG15-regulated, Tsg101-dependent pathway for rerouting proteins to the plasma membrane. This pathway is exploited by influenza glycoproteins along with other membrane proteins, such as CD40L, to traffic to the PM upon IFN induction.

budding (Bruce et al., 2010; Cox et al., 2000; Eisfeld et al., 2011). Our results predict that IAV must be able to either exploit host de-ISGylases or employ NS1 in order to prevent ISG15 levels from reaching a threshold to be able to overcome the inhibition imposed by IFN induction. Future work will determine whether or not that occurs.

EXPERIMENTAL PROCEDURES

Antibodies, Cell Lines, and Constructs

MDCK, Vero, A549, and HEK 293T cells were purchased from American Type Culture Collection and cultured. Serum containing IgG against A/WSN/33 influenza HA was from a transnuclear mouse generated in the laboratory. The antibody against the HA epitope was purchased from Roche (3F-10). Plasmid encoding PFO was provided by A. Johnson (Texas A&M University). Antibodies against Tsg101, Vps4, and IAV M1 were purchased from Abcam. GTPγS was purchased from Sigma-Aldrich. The construct for recombinant PFO and its purification have been described before (Sanyal et al., 2012; Flanagan et al., 2009). HA agarose beads were purchased from Roche, and protein A agarose beads were from RepliGen Bioprocessing. The generation of HA-Srt virus has been described before (Popp et al., 2012).

HA-Transport Assays and Virus Budding in PFO-Permeabilized Cells

MDCK cells were grown to 80%–90% confluency, infected with WSN/33/A virus for 5 hr, and labeled with [^{35}S]cysteine/methionine at 37°C in suspension. Labeled cells were treated with 0.1 μM PFO (in Hank's balanced salt solution [HBSS]) on ice as described above. Excess PFO was removed by dilution in HBSS and centrifugation. For measuring IAV trafficking and budding, ~2.5 × 10^6 PFO treated semi-intact cells were incubated with ~100 μg of concentrated MDCK cytosol in 50 μl and incubated at 37°C for 30 and 60 min. For all samples, cytosol preps used were normalized to total protein concentrations. At each time point, cell suspensions were centrifuged at 1,000 × *g* for 3 min in order to separate the pellet and supernatant fractions. The pellets were washed once with cold PBS and lysed (0.5% NP-40, 150 mM NaCl, 5 mM $MgCl_2$, and 25 mM Tris [pH 7.5]). The supernatants were diluted to 500 μl in PBS, centrifuged further at 2,000 rpm for 5 min in order to remove any contaminants, and treated with chicken erythrocytes in order to isolate released virus particles. HA was recovered with serum from transnuclear mouse immobilized on protein G sepharose beads. Immunoprecipitated material was resolved by SDS-PAGE and visualized by autoradiography. Chicken erythrocytes with adsorbed virions were lysed in resolving sample buffer and loaded directly for SDS-PAGE.

Designing CRISPR Target Sequence and Prediction of Potential Off-Target Effects

Potential target sequences for CRISPR interference were found with the rules outlined in Mali et al. (2013). The seed sequence preceding the PAM motif was found in the exon of Tsg101 as follows:Tsg101 target sequence, CTGTTCTGTTTTCAGGCCGAGG. Potential off-target effects of the seed sequence were confirmed with the NCBI *Homo sapiens* Nucleotide BLAST.

Procedure for Generating CRISPR RNA-Expressing Vector

The sense and antisense oligos were designed to incorporate into the restriction enzymatic site BbsI of pX330 bicistronic expression vector expressing Cas9 and synthetic single-guide RNA (Cong et al., 2013) as follows: sense oligo, caccgCTGTTCTGTTTTCAGGCCG; antisense oligo, aaacCGGCCTGA AAACAGAACAGc. The oligo DNAs were annealed, phosphorylated, and incorporated into pX330 vector linearized with BbsI restriction enzyme.

Limiting Dilution to Generate Tsg101 Knockout Cell Lines

A549 cells were transfected with the Tsg101-targeting pX330 with FuGENE6 reagent (Promega) according to the manufacturer's instructions. The cells were replated 12 hr after transfection to a 96-well plate at a density of 0.5 cells per well. The individual colonies were picked, and the expressions of Tsg101 were checked by immunoblotting.

Plaque Assay

Serial dilutions of supernatants from infected cells were overlaid on MDCK cells and incubated for 30 min. Cells were washed, and plaque media was added to the cells (MEM; 0.8% agar, 1 μg/ml trypsin) and placed at 37°C. Cells were fixed in 4% paraformaldehyde 48 hr after infections, and the agar plug was removed. Cells were blocked in 5% BSA and 1% goat serum and probed with anti-NP VHH54-biotin followed by streptavidin-HRP (GE Healthcare,

RPN1231V). Plaques were subsequently visualized with TrueBlue Peroxidase Substrate (Kirkegaard and Perry Laboratories, 50-78-02).

Immunodepletions of Tsg101 and Vps4

100 μl of concentrated cytosol from MDCK cells (500 μg protein) isolated by PFO treatments was subjected to control beads and anti-Vps4 or anti-Tsg101 immobilized on protein A sepharose beads. After incubation for 3 hr at 4°C, flowthrough fractions were collected from mock-depleted, Vps4-deficient, or Tsg101-deficient samples and subjected to immunoblotting in order to confirm depletion. GAPDH was used as a loading control in order to verify that depletion was specific. Immunodepleted cytosol was incubated with semi-intact cells in order to measure HA transport and virus budding as described before.

SUPPLEMENTAL INFORMATION

Supplemental Information contains Supplemental Results, Supplemental Experimental Procedures, and one figure and can be found with this article online at http://dx.doi.org/10.1016/j.chom.2013.10.011.

ACKNOWLEDGMENTS

This work was funded by the National Institutes of Health (RO1 grants AI033456 and AI087879 to H.L.P.) and Sanofi Pasteur (H.L.P.) and partially by the Center for Research on Influenza Pathogenesis (NIAID CEIRS contract HHSN266200700010C and NIAID grant U19 AI083025 to A.G.-S.). For technical assistance and discussions, the authors acknowledge Richard Cadagan, Fikadu Tafesse, Carla Guimaraes, and Lee Kim Swee.

Received: May 3, 2013
Revised: August 13, 2013
Accepted: October 7, 2013
Published: November 13, 2013

REFERENCES

Brass, A.L., Huang, I.-C., Benita, Y., John, S.P., Krishnan, M.N., Feeley, E.M., Ryan, B.J., Weyer, J.L., van der Weyden, L., Fikrig, E., et al. (2009). The IFITM proteins mediate cellular resistance to influenza A H1N1 virus, West Nile virus, and dengue virus. Cell *139*, 1243–1254.

Bruce, E.A., Medcalf, L., Crump, C.M., Noton, S.L., Stuart, A.D., Wise, H.M., Elton, D., Bowers, K., and Digard, P. (2009). Budding of filamentous and non-filamentous influenza A virus occurs via a VPS4 and VPS28-independent pathway. Virology *390*, 268–278.

Bruce, E.A., Digard, P., and Stuart, A.D. (2010). The Rab11 pathway is required for influenza A virus budding and filament formation. J. Virol. *84*, 5848–5859.

Chen, B.J., Leser, G.P., Jackson, D., and Lamb, R.A. (2008). The influenza virus M2 protein cytoplasmic tail interacts with the M1 protein and influences virus assembly at the site of virus budding. J. Virol. *82*, 10059–10070.

Cong, L., Ran, F.A., Cox, D., Lin, S., Barretto, R., Habib, N., Hsu, P.D., Wu, X., Jiang, W., Marraffini, L.A., and Zhang, F. (2013). Multiplex genome engineering using CRISPR/Cas systems. Science *339*, 819–823.

Cox, D., Lee, D.J., Dale, B.M., Calafat, J., and Greenberg, S. (2000). A Rab11-containing rapidly recycling compartment in macrophages that promotes phagocytosis. Proc. Natl. Acad. Sci. USA *97*, 680–685.

Diaz, L., Cassella, J., Bonavia, A., Duan, R., Santos, D., Fesseha, Z., Goldblatt, M., and Kinch, M. (2009). Recruitment of the TSG101/ESCRT-I Machinery in Host Cells by Influenza Virus: Implications for Broad-Spectrum Therapy. Antiviral Res. *82*, A71.

Eisfeld, A.J., Kawakami, E., Watanabe, T., Neumann, G., and Kawaoka, Y. (2011). RAB11A is essential for transport of the influenza virus genome to the plasma membrane. J. Virol. *85*, 6117–6126.

Ernst, R., Claessen, J.H.L., Mueller, B., Sanyal, S., Spooner, E., van der Veen, A.G., Kirak, O., Schlieker, C.D., Weihofen, W.A., and Ploegh, H.L. (2011). Enzymatic blockade of the ubiquitin-proteasome pathway. PLoS Biol. *8*, e1000605.

Flanagan, J.J., Tweten, R.K., Johnson, A.E., and Heuck, A.P. (2009). Cholesterol exposure at the membrane surface is necessary and sufficient to trigger perfringolysin O binding. Biochemistry *48*, 3977–3987.

Freed, E.O. (2004). HIV-1 and the host cell: an intimate association. Trends Microbiol. *12*, 170–177.

Frias-Staheli, N., Giannakopoulos, N.V., Kikkert, M., Taylor, S.L., Bridgen, A., Paragas, J., Richt, J.A., Rowland, R.R., Schmaljohn, C.S., Lenschow, D.J., et al. (2007). Ovarian tumor domain-containing viral proteases evade ubiquitin- and ISG15-dependent innate immune responses. Cell Host Microbe *2*, 404–416.

Hanson, P.I., and Cashikar, A. (2012). Multivesicular body morphogenesis. Annu. Rev. Cell Dev. Biol. *28*, 337–362.

Hsiang, T.-Y., Zhao, C., and Krug, R.M. (2009). Interferon-induced ISG15 conjugation inhibits influenza A virus gene expression and replication in human cells. J. Virol. *83*, 5971–5977.

Hwang, W.Y., Fu, Y., Reyon, D., Maeder, M.L., Tsai, S.Q., Sander, J.D., Peterson, R.T., Yeh, J.-R.J., and Joung, J.K. (2013). Efficient genome editing in zebrafish using a CRISPR-Cas system. Nat. Biotechnol. *31*, 227–229.

Jouvenet, N., Simon, S.M., and Bieniasz, P.D. (2011). Visualizing HIV-1 assembly. J. Mol. Biol. *410*, 501–511.

Karlas, A., Machuy, N., Shin, Y., Pleissner, K.-P., Artarini, A., Heuer, D., Becker, D., Khalil, H., Ogilvie, L.A., Hess, S., et al. (2010). Genome-wide RNAi screen identifies human host factors crucial for influenza virus replication. Nature *463*, 818–822.

Lee, M.C.S., and Miller, E.A. (2007). Molecular mechanisms of COPII vesicle formation. Semin. Cell Dev. Biol. *18*, 424–434.

Malakhov, M.P., Malakhova, O.A., Kim, K.I., Ritchie, K.J., and Zhang, D.-E. (2002). UBP43 (USP18) specifically removes ISG15 from conjugated proteins. J. Biol. Chem. *277*, 9976–9981.

Mali, P., Yang, L., Esvelt, K.M., Aach, J., Guell, M., DiCarlo, J.E., Norville, J.E., and Church, G.M. (2013). RNA-guided human genome engineering via Cas9. Science *339*, 823–826.

Martin-Serrano, J., and Neil, S.J.D. (2011). Host factors involved in retroviral budding and release. Nat. Rev. Microbiol. *9*, 519–531.

Martin-Serrano, J., Zang, T., and Bieniasz, P.D. (2001). HIV-1 and Ebola virus encode small peptide motifs that recruit Tsg101 to sites of particle assembly to facilitate egress. Nat. Med. *7*, 1313–1319.

Okumura, A., Lu, G., Pitha-Rowe, I., and Pitha, P.M. (2006). Innate antiviral response targets HIV-1 release by the induction of ubiquitin-like protein ISG15. Proc. Natl. Acad. Sci. USA *103*, 1440–1445.

Okumura, A., Pitha, P.M., and Harty, R.N. (2008). ISG15 inhibits Ebola VP40 VLP budding in an L-domain-dependent manner by blocking Nedd4 ligase activity. Proc. Natl. Acad. Sci. USA *105*, 3974–3979.

Popp, M.W., Antos, J.M., Grotenbreg, G.M., Spooner, E., and Ploegh, H.L. (2007). Sortagging: a versatile method for protein labeling. Nat. Chem. Biol. *3*, 707–708.

Popp, M.W.-L., Antos, J.M., and Ploegh, H.L. (2009). Site-specific protein labeling via sortase-mediated transpeptidation. Curr Protoc Protein Sci *Chapter 15*, Unit15.3.

Popp, M.W.-L., Karssemeijer, R.A., and Ploegh, H.L. (2012). Chemoenzymatic site-specific labeling of influenza glycoproteins as a tool to observe virus budding in real time. PLoS Pathog. *8*, e1002604.

Razi, M., and Futter, C.E. (2006). Distinct roles for Tsg101 and Hrs in multivesicular body formation and inward vesiculation. Mol. Biol. Cell *17*, 3469–3483.

Rossman, J.S., and Lamb, R.A. (2011). Influenza virus assembly and budding. Virology *411*, 229–236.

Rossman, J.S., Jing, X., Leser, G.P., and Lamb, R.A. (2010). Influenza virus M2 protein mediates ESCRT-independent membrane scission. Cell *142*, 902–913.

Ruigrok, R.W.H., Barge, A., Durrer, P., Brunner, J., Ma, K., and Whittaker, G.R. (2000). Membrane interaction of influenza virus M1 protein. Virology *267*, 289–298.

Sanyal, S., Claessen, J.H.L., and Ploegh, H.L. (2012). A viral deubiquitylating enzyme restores dislocation of substrates from the endoplasmic reticulum (ER) in semi-intact cells. J. Biol. Chem. *287*, 23594–23603.

Schmitt, A.P., and Lamb, R.A. (2005). Influenza virus assembly and budding at the viral budozone. Adv. Virus Res. *64*, 383–416.

Seo, E.J., and Leis, J. (2012). Budding of Enveloped Viruses: Interferon-Induced ISG15-Antivirus Mechanisms Targeting the Release Process. Adv. Virol. *2012*, 532723.

Shapira, S.D., Gat-Viks, I., Shum, B.O.V., Dricot, A., de Grace, M.M., Wu, L., Gupta, P.B., Hao, T., Silver, S.J., Root, D.E., et al. (2009). A physical and regulatory map of host-influenza interactions reveals pathways in H1N1 infection. Cell *139*, 1255–1267.

Skaug, B., and Chen, Z.J. (2010). Emerging role of ISG15 in antiviral immunity. Cell *143*, 187–190.

Tafesse, F.G., Sanyal, S., Ashour, J., Guimaraes, C.P., Hermansson, M., Somerharju, P., and Ploegh, H.L. (2013). Intact sphingomyelin biosynthetic pathway is essential for intracellular transport of influenza virus glycoproteins. Proc. Natl. Acad. Sci. USA *110*, 6406–6411.

Tsurudome, M., Glück, R., Graf, R., Falchetto, R., Schaller, U., and Brunner, J. (1992). Lipid interactions of the hemagglutinin HA2 NH2-terminal segment during influenza virus-induced membrane fusion. J. Biol. Chem. *267*, 20225–20232.

Wagner, K.U., Krempler, A., Qi, Y., Park, K., Henry, M.D., Triplett, A.A., Riedlinger, G., Rucker, E.B., III, and Hennighausen, L. (2003). Tsg101 is essential for cell growth, proliferation, and cell survival of embryonic and adult tissues. Mol. Cell. Biol. *23*, 150–162.

Watanabe, R., and Lamb, R.A. (2010). Influenza virus budding does not require a functional AAA+ ATPase, VPS4. Virus Res. *153*, 58–63.

White, J.J., Matlin, K.K., and Helenius, A.A. (1981). Cell fusion by Semliki Forest, influenza, and vesicular stomatitis viruses. J. Cell Biol. *89*, 674–679.

Yuan, W., and Krug, R.M. (2001). Influenza B virus NS1 protein inhibits conjugation of the interferon (IFN)-induced ubiquitin-like ISG15 protein. EMBO J. *20*, 362–371.

Zhao, C., Hsiang, T.-Y., Kuo, R.-L., and Krug, R.M. (2010). ISG15 conjugation system targets the viral NS1 protein in influenza A virus-infected cells. Proc. Natl. Acad. Sci. USA *107*, 2253–2258.

Zhao, C., Collins, M.N., Hsiang, T.-Y., and Krug, R.M. (2013). Interferon-induced ISG15 pathway: an ongoing virus-host battle. Trends Microbiol. *21*, 181–186.